scientific reports

Check for updates

OPEN

Applications of Cattaneo–Christov fluxes on modelling the boundary value problem of Prandtl fluid comprising variable properties

Umar Nazir[1], Muhammad Sohail[1]✉, Umair Ali[1], El-Sayed M. Sherif[2], Choonkil Park[3]✉, Jung Rye Lee[4], Mahmoud M. Selim[5,6] & Phatiphat Thounthong[7]

Stretched flows have numerous applications in different industrial, biomedical and engineering processes. Current research is conducted to examine the flow phenomenon of Prandtl fluid model over a moveable surface. The phenomenon of mass and thermal transportation is based on generalized theory of Cattaneo–Christov which considers the involvement of relaxation times. In addition to these, variable characteristics of thermal conductivity and diffusion coefficient are considered as a function of temperature. The physical problem in Cartesian coordinate system is modeled via boundary layer theory which yields a coupled system of partial differential equations. Group scaling transportation is applied to model these PDEs system. The converted equations have been approximated via optimal homotopic scheme. The efficiency and validity of used approach has been shown by computing the error analysis and establishing a comparative study. It is noted that the enhancement in magnetic parameter plays a controlling role for velocity field and it augment the concentration and temperature fields. Furthermore, increase in thermal relaxation parameter and Prandtl number maintains the fluid temperature.

The rheology of non-Newtonian fluids has complex nature and it cannot be exactly described by the stress–strain relatively as proposed by Newton. Non-Newtonian materials appear frequently, and it has applications in different mechanisms. One of the important non-Newtonian fluid is Prandtl fluid model[1] which is describes the following constitutive relation

$$\tau = \left[A\left(\frac{\partial v}{\partial y}\right)^2 + A\left(\frac{\partial u}{\partial y}\right)^2\right]^{-\frac{1}{2}} \sin^{-1}\left[\frac{1}{C}\left[\left(\frac{\partial u}{\partial y}\right)^2 + \left(\frac{\partial v}{\partial y}\right)^2\right]^{\frac{1}{2}} \frac{\partial u}{\partial y}\right]$$

where "τ" denotes the stress tensor for Prandtl model, ""A and C"" are material parameters. The classification of fluids (non-Newtonian) is based on their behaviors and shear thinning category of fluids is considered as important in fluids. The model related to Prandtl fluid is known as a shear thinning liquid. Human blood, paint, blood, industrial and polymers products are examples of Prandtl fluid. This kind of liquid performs like a non-Newtonian fluid. Several applications of such non-Newtonion fluid in sugar production, cement industry, making shampoos and drilling muds etc. Several researchers have worked on this model by considering the different physical effects under different circumstances and assumptions. For instance, Hamid et al.[1] worked on unsteady natural convection flow of Prandtl model over a moveable surface. They considered the chemical reaction,

[1]Department of Applied Mathematics and Statistics, Institute of Space Technology, P.O. Box 2750, Islamabad 44000, Pakistan. [2]Mechanical Engineering Department, College of Engineering, King Saud University, P.O. Box 800, Al-Riyadh 11421, Saudi Arabia. [3]Research Institute for Natural Sciences, Hanyang University, Seoul 04763, Korea. [4]Department of Data Science, Daejin University, Pocheon, Kyunggi 11159, Korea. [5]Department of Mathematics, Al-Aflaj College of Science and Humanities Studies, Prince Sattam Bin Abdulaziz University, Al-Aflaj 710-11912, Saudi Arabia. [6]Department of Mathematics, Suez Faculty of Science, Suez University, Suez 34891, Egypt. [7]Department of Teacher Training in Electrical Engineering, Faculty of Technical Education, Renewable Energy Research Centre, King Mongkut's University of Technology North Bangkok, 1518 Pracharat 1 Road, Bangsue, Bangkok 10800, Thailand. ✉email: muhammad_sohail111@yahoo.com; baak@hanyang.ac.kr

radiation and magnetohydrodynamic influences. They studied the mass and thermal transport on Prandtl model by applying the boundary layer theory on the associated conservation laws. They obtained the solution via numerical method namely "Crank-Nicolson" coded in MATLAB symbolic computational package. They recorded that augmenting volume of unsteadiness parameter upsurges the momentum, thermal and concentration fields. Rajesh and Rajasekhara Gowd[2] discussed the rheology of Prandtl fluid during the transport of solute particles and thermal energy past a porous vertical channel. They also considered thermal radiation phenomena along with magnetic field. Later on, the governing model is transformed into PDEs by appropriate substitution and then solved analytically. They found a rise in velocity field against gravitational parameters. Eldabe et al.[3] focused on peristaltic motion of Prandtl liquid considering chemical reaction and electrical conductivity (variable) obeying the mixed convection in symmetric channel. They used differential transform procedure to tackle the resulting equation. They illustrated the solutions through graphs. They noticed the decline in pressure profile against chemical reaction parameters. Flow of Prandtl model over a rotating slippery sheet with convective condition, radiation and concentration dependent diffusion coefficient was investigated by Sajid et al.[4] They recorded the amplification in thermal profile for radiation parameter and decline in velocity field against rotating parameter. Reddy et al.[5] modeled the compartment of modified heat flux. They handled the resulting equations as a numerically. They reported that velocity profile escalates against elastics and Prandtl fluid parameters Transient numerical solution for Prandtl model in rotating surface was discussed by Le et al.[6]. They reported the phenomenon of bifurcation. Transportation of heat energy as well as mass has significant application in different field of applied sciences. Ahmad et al.[7] used non-Fourier's model to study the heating effects on micropolar fluid over a hot surface. They assumed the slip conditions, thermal radiation and magneto-hydrodynamic effect in their research. Numerically they handled the resulting modeled expression. They studied the entropy analysis and recorded that mounting value of material parameter and Reynolds number entrances the entropy generation. Tassadiq[8] studied the homotopic solution for micropolar hybrid nanofluid model with dissipation and Joule heating effects and they solved the modeled equations with the help of numerical approach. Through graphical solution, they predicted the decline in velocity filed against Hartmann number and micropolar parameters. Ahmad et al.[9] reported the phenomenon of shallow wave dispersive equation arising in mathematical physics. They presented the graphical analysis of two methods. Tulu and Ibrahim[10] studied the use of CNT-Ethylene Glycol to enhance the thermal transport over a rotating stretchable disc with modified heat flux model. They solved the nonlinear transport equation numerically. Through graphs they recorded the behavior of solution against numerous emerging parameters. They noticed that radial stretching of the disc improves the cooling effect which is beneficial to control the thermal stability of the system. Numerical solution of Jeffrey liquid model is captured by Mabood et al.[11] with heat transport phenomenon. Graphically they plotted the behavior of parameters for the assisting and opposing flow situations. They mentioned the decline in temperature field against Deborah number. Finite element analysis is applied to study the double diffusion theories on Casson model by Ali et al.[12]. They noticed the decrease in primary and secondary velocity against magnetic parameter and fluid parameter, where, rise in concentration and thermal profile is seen. Khan et al.[13] presented the theoretical analysis on thermal transport with the inclusion of different nanoparticles. They noticed the depreciation in thermal field for Prandtl number. Heat transport in Oldroyd-B model over elastic surface in inspected by Ramana et al.[14] numerically. Jakeer et al.[15] considered finite volume approach to study the thermal transport in lid-driven porous cavity. They plotted the streamlines against flow controlling parameters. Nadeem et al.[16] modeled the transport phenomenon of thermal energy in Newtonian liquid in the attendance of non-Fourier's theory. They investigated this transport phenomenon past heated surface via Optimal HAM approach. Ahmad et al.[17] scrutinized theory related to the non-Fourier in micropolar fluid considering the presence of heat absorption. They used the role nanoparticles in micropolar fluid and they also simulated the entropy generation mechanism. Ahmad et al.[18] simulated the features of thermal energy and solute particles in micropolar involvement of nanoparticles and hybrid nanoparticles in base fluid called water. They used the stretching heated surface formeasurement of considering features in the presence of non-Fourier's theory along with activation energy. Ahmad and Nadeem[19] analyzed the role of non-Fourier's law in the energy equation along with slip conditions (Thomson and Troian). Several recently studied contribution are reported in[20–26] and references therein.

Available literature tells that no study is conducted with variable thermo-physical properties for 3D Prandtl model with double diffusion theories. This model covers all aspects which are missing in published work. The adjustment of present model is considered into following: Literature with detailed description is performed in "Introduction" section, fluid rheology with heat and mass transport phenomenon are listed in "Mathematical formulation of transport problem" section with dimensionless equations, "Numerical method for solution" section contains the methodology, "Discussion and analysis on graphical and tabular results" and "Concluding key points" sections describe the detailed discussion on graphical outcomes with conclusion.

Mathematical formulation of transport problem

Steady incompressible flow of Prandtl fluid heat and mass transport is considered in this project as shown in Fig. 1. The stretching of sheet is responsible to maintain the flow. The sheet is stretched in x- and y- direction respectively and flow region is $z \geq 0$. The direction of uniform magnetic field is considered to normal of x- and y- directions as shown in Fig. 1. The characteristics of heat energy and diffusion of fluid particles are reported under the action of timrelaxations. The concept fluxes (heat and mass) including relaxation times are

$$\boldsymbol{Q} + \alpha_1 \left[\frac{\partial \boldsymbol{Q}}{\partial t} + \boldsymbol{V} \cdot \nabla \boldsymbol{Q} - \boldsymbol{Q} \cdot \nabla \mathbf{V} + (\nabla \cdot \mathbf{V}) \mathbf{Q} \right] = -K(T) \nabla \mathrm{T}, \tag{1}$$

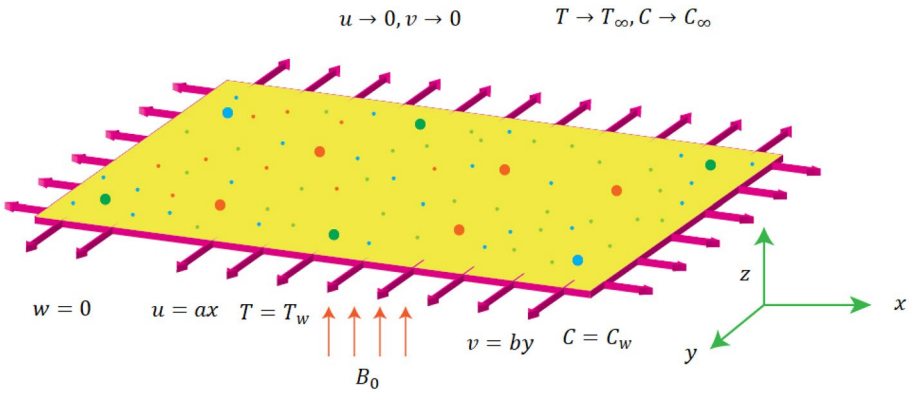

Figure 1. Flow diagram of Prandtl fluid.

$$\boldsymbol{J} + \alpha_2 \left[\frac{\partial \boldsymbol{J}}{\partial t} + \boldsymbol{V} \cdot \nabla \mathbf{J} - \mathbf{J} \cdot \nabla \mathbf{V} + (\nabla \cdot \mathbf{V})\mathbf{J} \right] = -D(T)\nabla \mathbf{J}. \tag{2}$$

Using incompressibility and steady flow assumptions, we get

$$\boldsymbol{Q} + \alpha_1 [\boldsymbol{V} \cdot \nabla \mathbf{Q} - \mathbf{Q} \cdot \nabla \mathbf{V}] = -K(T)\nabla \mathrm{T}, \tag{3}$$

$$\boldsymbol{J} + \alpha_2 [\boldsymbol{V} \cdot \nabla \mathbf{J} - \mathbf{J} \cdot \nabla \mathbf{V}] = -D(T)\nabla \mathbf{J}. \tag{4}$$

where "$\boldsymbol{Q}$" is heat flux, "$\boldsymbol{V}$" represents velocity field, "$K(T)$" the thermal conductivity, "$\boldsymbol{J}$" the mass flux, "D(T)" the diffusion coefficient, "α_1" and "α_2" are thermal and concentration relaxation times using the boundary layer theory the conservation laws for Prandtl model takes the form

$$\frac{\partial v}{\partial y} + \frac{\partial w}{\partial z} + \frac{\partial u}{\partial x} = 0, \tag{5}$$

$$\left(v\frac{\partial}{\partial y} + w\frac{\partial}{\partial z} + u\frac{\partial}{\partial x} \right) u = \frac{A}{C}\delta \frac{\partial^2 u}{\partial z^2} + \delta \frac{A}{2C^3} \left(\frac{\partial u}{\partial z} \right)^2 \frac{\partial^2 u}{\partial z^2} - \frac{\sigma}{\rho} u B_0^2, \tag{6}$$

$$\left(v\frac{\partial}{\partial y} + w\frac{\partial}{\partial z} + u\frac{\partial}{\partial x} \right) v = \frac{A}{C}\delta \frac{\partial^2 v}{\partial z^2} + \delta \frac{A}{2C^3} \left(\frac{\partial v}{\partial z} \right)^2 \frac{\partial^2 v}{\partial z^2} - \frac{\sigma v B_0^2}{\rho}, \tag{7}$$

$$\begin{aligned} uT_x + vT_y + wT_z + \alpha_1 \begin{bmatrix} \left(v\frac{\partial}{\partial y} + w\frac{\partial}{\partial z} + u\frac{\partial}{\partial x} \right) uT_x + \left(v\frac{\partial}{\partial y} + w\frac{\partial}{\partial z} + u\frac{\partial}{\partial x} \right) vT_y \\ + \left(v\frac{\partial}{\partial y} + w\frac{\partial}{\partial z} + u\frac{\partial}{\partial x} \right) wT_z + 2uvT_{xy} + 2vwT_{yz} \\ + 2uwT_{xz} + u^2 T_{xx} + v^2 T_{yy} + w^2 T_{zz} \end{bmatrix} \\ = \nabla [K(T)\nabla \mathrm{T}], \end{aligned} \tag{8}$$

$$\begin{aligned} uC_x + vC_y + wC_z + \alpha_2 \begin{bmatrix} \left(v\frac{\partial}{\partial y} + w\frac{\partial}{\partial z} + u\frac{\partial}{\partial x} \right) uC_x + \left(v\frac{\partial}{\partial y} + w\frac{\partial}{\partial z} + u\frac{\partial}{\partial x} \right) vC_y \\ + \left(v\frac{\partial}{\partial y} + w\frac{\partial}{\partial z} + u\frac{\partial}{\partial x} \right) wC_z + 2uvC_{xy} + 2vwC_{yz} \\ + 2uwC_{xz} + u^2 C_{xx} + v^2 C_{yy} + w^2 C_{zz} \end{bmatrix} \\ = \nabla [\mathrm{D(T)}\nabla \mathrm{C}]. \end{aligned} \tag{9}$$

Boundary conditions (BCs) are necessary to compute the solution of derived problem and BCs of present model are

$$\begin{cases} u = U_w = ax, v = V_w = by, w = 0, T = T_w, C = C_w \text{ at } z = 0. \\ u \to 0, v \to 0, T \to T_\infty, C \to C_\infty \text{ for } z \to \infty. \end{cases} \tag{10}$$

With the use of following similarity variables governing laws with associated conditions reduces to

$$\begin{cases} u = axf'(\xi), v = ayg'(\xi), w = -(a\delta)^{\frac{1}{2}}\left[f(\xi)+g(\xi)\right], \\ \theta(\xi) = \frac{T-T_\infty}{T_w-T_\infty}, \phi(\xi) = \frac{C-C_\infty}{C_w-C_\infty}, \xi = \left(\frac{a}{\delta}\right)^{\frac{1}{2}} z. \end{cases} \tag{11}$$

$$\beta_1 f'''(\xi) + \left[f(\xi)+g(\xi)\right]f''(\xi) - \left[f'(\xi)\right]^2 + \beta_2 f'''(\xi)\left[f''(\xi)\right]^2 - Mf'(\xi) = 0, \tag{12}$$

$$\beta_1 g'''(\xi) + \left[f(\xi)+g(\xi)\right]g''(\xi) - \left[g'(\xi)\right]^2 + \beta_2 g'''(\xi)\left[g''(\xi)\right]^2 - Mg'(\xi) = 0, \tag{13}$$

$$\begin{aligned} &\frac{1}{Pr}[1+\epsilon_1\theta(\xi)]\theta''(\xi) + \left[f(\xi)+g(\xi)\right]\theta'(\xi) \\ &\quad - \delta_1\left[f(\xi)+g(\xi)\left(f'(\xi)+g'(\xi)\right)\theta'(\xi) + \left(f(\xi)+g(\xi)\right)^2\theta''(\xi)\right] = 0, \end{aligned} \tag{14}$$

$$\begin{aligned} &\frac{1}{Sc}[1+\epsilon_2\theta(\xi)]\phi''(\xi) + \left[f(\xi)+g(\xi)\right]\phi'(\xi) \\ &\quad - \delta_2\left[f(\xi)+g(\xi)\left(f'(\xi)+g'(\xi)\right)\phi'(\xi) + \left(f(\xi)+g(\xi)\right)^2\phi''(\xi)\right] = 0, \end{aligned} \tag{15}$$

$$\begin{cases} \xi = 0, g = f = 0, f' = 1, g' = \alpha, \theta = \phi = 1, \\ \xi = \infty, f' = g' = 0, \theta = \phi = 0. \end{cases} \tag{16}$$

where "β_1" presents Prandtl fluid parameter, "β_2" the elastic parameter, "α" ratio parameter, "M" the magnetic parameter, "Pr" the Prandtl number, "Sc" the Schmidt number, "ϵ_1 and ϵ_2" are small parameters and "δ_1 and δ_2" denotes thermal and concentration relaxation times.

Physical quantities. To understand the several practical applications, the study of stress, heat and mass transfer rate have significant use. The empirical relations of these quantities are

$$C_{fx} = \frac{\tau_{zx}}{\rho(U)^2}, C_{fy} = \frac{\tau_{zy}}{\rho(V_w)^2},$$

$$Nu_x = -\frac{xQ_w}{K(T)(T_w - T_\infty)}, Sh_x = -\frac{xJ_w}{D(T)(C_w - C_\infty)}, U_w = ax, V = by, \tag{17}$$

where $\tau_{zx} = \frac{A}{C}u_z + \frac{A}{6C^3}(u_z)^3|_{z=0}, \tau_{zy} = \frac{A}{C}v_z + \frac{A}{6C^3}(v_z)^3|_{z=0}, Q_w = -K(T)\nabla T,$

$$J_w = -D(T)\nabla C,$$

the dimensionless form is

$$C_{fx} = \beta_1 f'''(\xi) + \beta_2\left[f'''(\xi)\right]^2|_{\xi=0},\ C_{fy} = \beta_1 g'''(\xi) + \beta_2\left[g'''(\xi)\right]^2|_{\xi=0}, \tag{18}$$

$$Hu_x = -[1+\epsilon_1\theta(\xi)]\theta'(0),\ Lh_x = -[1+\epsilon_2\theta(\xi)]\phi'(0). \tag{19}$$

Numerical method for solution

In this section, comprehensive literature survey on the considered topic is presented and "Mathematical formulation of transport problem" section comprises the mathematical form of the considered model-along with associated conditions. The current approach has ability to simulate complex flow problems. Several analytical and numerical schemes exist for the solution of differential equations. Here, optimal homotopy scheme is proposed for the solution. This procedure requires the linear operators and initial guess for the start of algorithm. These are

$$\begin{cases} L_F = \frac{D^3}{D\xi^3} - \frac{D}{D\xi}, L_G = \frac{D^3}{D\xi^3} - \frac{D}{D\xi}, \\ L_T = \frac{D^2}{D\xi^2} - 1, L_C = \frac{D^2}{D\xi^2} - 1, \end{cases} \tag{20}$$

$$\begin{cases} f_a(\xi) = 1 - e^{-\xi}, g_a = \alpha\left[1 - e^{-\xi}\right], \\ \theta_a(\xi) = e^{-\xi}, \phi_a(\xi) = e^{-\xi}, \end{cases} \tag{21}$$

The operators in Eq. (20) obey

$$L_F\left[\beta_1 + \beta_2 e^{-\xi} + \beta_3 e^{\xi}\right] = 0,$$

$$L_G\left[\beta_4 + \beta_5 e^{-\xi} + \beta_6 e^{\xi}\right] = 0,$$

Approximate Order (n)	δ_n^f	δ_n^g	δ_n^θ	δ_n^ϕ
2	0.00004268	6.9894×10^{-6}	0.00001112	0.0024046
4	1.09621×10^{-6}	6.79463×10^{-7}	1.23295×10^{-6}	0.0003176
8	6.94405×10^{-10}	1.68247×10^{-8}	1.71512×10^{-8}	0.00003448
12	1.45543×10^{-11}	8.02786×10^{-10}	6.00118×10^{-10}	6.61207×10^{-6}
16	1.73202×10^{-13}	2.49836×10^{-11}	1.87111×10^{-11}	1.60319×10^{-7}
20	9.10536×10^{-15}	1.01889×10^{-12}	1.3158×10^{-13}	4.48226×10^{-7}

Table 1. Computation of averaged squared residuals errors of velocity, temperature, and concentration solution.

$$L_T\left[\beta_7 e^{-\xi} + \beta_8 e^{\xi}\right] = 0,$$

$$L_C\left[\beta_9 e^{\xi} + \beta_{10} e^{-\xi}\right] = 0,$$

where $\beta_m (m = 1, 2, \ldots, 10)$ are unknowns.

Using the concepts of minimization of average squared residual error[21]

$$e_m^f = \frac{1}{i+1}\sum_{r=0}^{i}\left[M_f\left(\sum_{l=0}^{m}\hat{f}(\xi), \sum_{l=0}^{m}\hat{g}(\xi)\right)\right]^2,$$

$$e_m^g = \frac{1}{i+1}\sum_{r=0}^{i}\left[M_g\left(\sum_{l=0}^{m}\hat{f}(\xi), \sum_{l=0}^{m}\hat{g}(\xi)\right)\right]^2,$$

$$e_m^\theta = \frac{1}{i+1}\sum_{r=0}^{i}\left[M_\theta\left(\sum_{l=0}^{m}\hat{f}(\xi), \sum_{l=0}^{m}\hat{g}(\xi), \sum_{l=0}^{m}\hat{\theta}(\xi)\right)\right]^2,$$

$$e_m^\phi = \frac{1}{i+1}\sum_{r=0}^{i}\left[M_\phi\left(\sum_{l=0}^{m}\hat{f}(\xi), \sum_{l=0}^{m}\hat{g}(\xi), \sum_{l=0}^{m}\hat{\theta}(\xi), \sum_{l=0}^{m}\hat{\phi}(\xi)\right)\right]^2,$$

where

$$e_m^t = e_m^f + e_m^g + e_m^\theta + e_m^\phi.$$

The optimal values at 3rd order are $H_f = -1.125554, H_g = -0.67757434, H_\theta = -1.00771259, H_\phi = -0.66544386$, by fixing the involved parameters as $Sc = 0.5, Pr = 1.0, \alpha = 0.4, \beta_1 = 0.5, \beta_2 = 0.6, M = 0.1, \delta_1 = 0.1, \delta_2 = 0.3, \epsilon_1 = 0.1, \epsilon_2 = 0.2$. Table 1 is prepared to notice the error analysis against higher order approximations.

Discussion and analysis on graphical and tabular results

The 3D flow situation of Prandtl fluid subjected to magnetic field under the action of Cattaneo–Christov heat flux is performed past a stretched surface. The variable properties called temperature dependent concentration and thermal conductivity are involved via slip conditions. This physical complex model is numerically simulated by numerical approach. The graphical simulations of heat energy, concentration and motion of fluid particles are conducted through graphs and tables while these simulations are given below:

Simulations of flow phenomenon versus physical parameters. The parameter called magnetic number captures features of Prandtl liquid under the action of non-Fourier's model using variable properties in the existence of mass and heat transport. The phenomenal role of M on x-and y-directions of velocities are illustrated by Figs. 2 and 5. The retardation force is generated in motion of fluid particles due to input of M and this retardation makes slow in speed of fluid particles. Actually, the action of magnetic field generates frictional force called opposing force (Lorentz force) in Eqs. (12) and 13. The Lorentz forces in y- and x-directions of momentum equations are $-Mf'(\xi)$ and $Mg'(\xi)$ in Eqs. (12) and (13) respectively. Moreover, constant strength of magnetic field is taken along vertical of heated surface. The direction of magnetic field is applied against the direction of flow and this happening creates resistance during the flow of fluid particles. Hence, Lorentz forces are negative force which is opposite to direction of flow. Therefore, secondary and primary velocities become slow down due to large integration of magnetic number. The representation of β_1 called Prandtl fluid parameter on secondary and primary velocities is delineated by Figs. 3 and 6. The parameter (β_1) is appeared in the current model due to tensor of Prandt fluid. The direct relation is found between the flow of fluid particles and β_1. An increment in

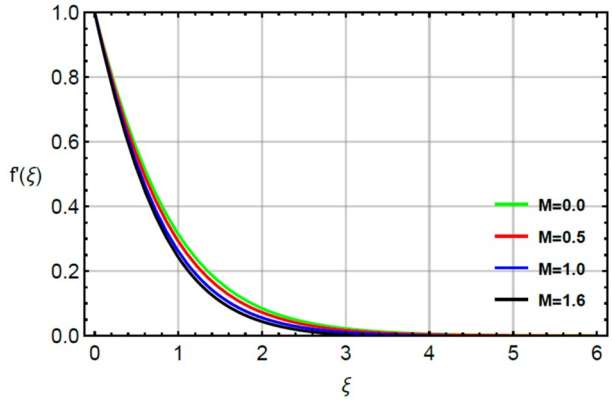

Figure 2. Character of M on f'.

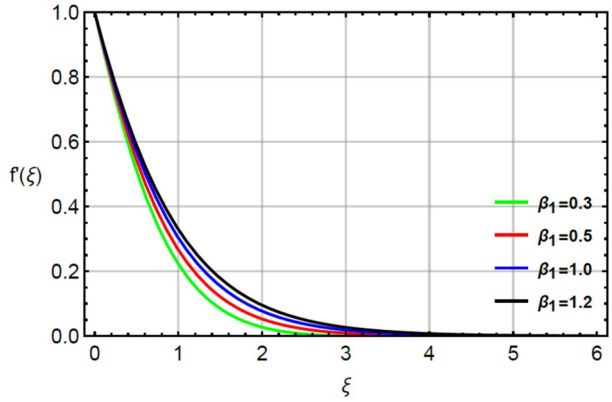

Figure 3. Character of β_1 on f'.

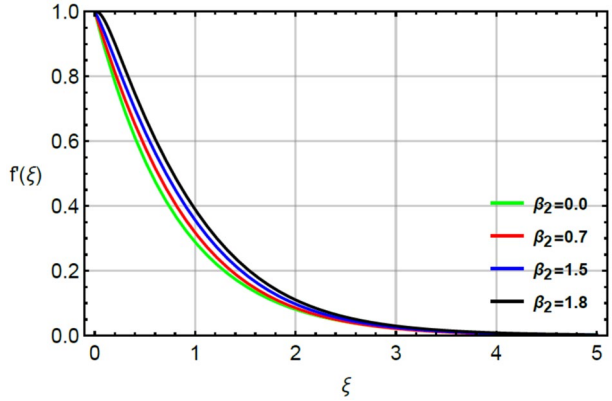

Figure 4. Character of β_2 on f'.

β_1 brings the enhancement in motion of fluid particles. Hence, velocities are increased versus the large values of β_1. Figures 4 and 7 portray the character of elastic parameter on the primary and secondary flows. To obtain the desired results of β_2, the range of $0.4 \leq \beta_2 \leq 1.8$ is considered. It can be found that for enhancing the values β_2 results profiles of velocities in y-and x-directions are enhanced. This type of situation is validated for large values of β_2 makes increment in viscosity of fluid. By the definition of elastic parameter, it has direct relation against the dynamic viscosity of fluid. The viscosity of fluid is reduced when elastic parameter is increased. Hence, the role of elastic parameter accelerates the motion in fluid particles.

Figure 8 plots the role α on g'. It is estimated that from outcome sketch flow of fluid particles in y-and x-directions become enhanced by large values of α. Moreover, viscosity of fluid becomes decrease by applying the increment of α. So, less viscosity is generated for large values of α and secondary and primary velocities are enhanced. The ratio number is considered as ratio of horizontal movement and vertical movement. The motion of fluid particles is acerbated due to motion of elastic heated surface. Meanwhile, ration parameter plays a vital impact to maximize the motion in fluid particles.

Simulations of heat energy versus physical parameters. The simulations of thermal energy are captured by variation of parameters called Prandtl (Pr), very small (ϵ_1) and thermal relaxation (δ_1) by Figs. 9, 10 and 11. Figure 9 captures the variation in thermal energy with applying the large values of ϵ_1. It is estimated that ϵ_1 is appeared due to role of changing of thermal conductivity with respect to temperature in dimensionless energy equation while the appearance of ϵ_1 decides the role of constant and variable thermal conductivities. From the Fig. 9, it can be clearly seen that enhancement in thermal energy is investigated versus large values of ϵ_1. This enhancement in thermal energy is happened because ϵ_1 has direct relation versus temperature in temperature dependent thermal conductivity model. So, this direct relation generates maximum heat energy via large values of ϵ_1. The parameter related to ϵ_1 is occurred due to variable thermal conductivity in energy equation (dimensionless). This parameter treats as linear function in thermal energy and an enhancement in ϵ_1 results increase the random motion of fluid particles due to temperature gradient. An increment in random motion of fluid particles correspondences increment in heat energy of fluid particles is happened. Hence, temperature enhances. Figure 10 indicates the characterization of thermal energy with higher values of Pr. As, Pr discusses the dual behavior of boundary layers regarding moment and thermal layers during the flow of fluid at boundary of the sheet. Actually, inverse relation between thermal layer and Pr. So, layers regarding thermal energy becomes declined versus the large values of Pr. Hence, increment in Pr results the reduction in thermal energy. Physically, Prandtl is considered as a fractional between the momentum boundary and thermal boundary layers. By the definition of Pr, layers regarding thermal are based on variation of Pr whereas thickness of thermal layers are increased versus the enlargement in Pr. The term regarding thermal relaxation parameter is developed using concept of non-Fourier's law in energy equation as well as in concentration equation. The appearance of δ_1 decides the role of non-Fourier's and Fourier's laws in present flow model while the appearance of δ_1 is simulated by Fig. 11. From this figure, layers regarding thermal energy attain less temperature. Consequently, temperature decreases with respect to large values of δ_1. In physical view, the term related to relaxation means reappearance of system into equilibrium condition and every process of relaxation are considered as a relaxation time. The large values of δ_1 reveals an enhancement in capability of Prandtl fluid to return the equilibrium state while this happening brings the minimizing variation in thermal state of Prandtl fluid.

Simulations of concentration versus physical parameters. Figures 12, 13 and 14 illustrate the influences of concentration with respect to variation of Sc, ϵ_2 and δ_2. Figure 12 conducts the role of Sc on the curves of concentration. The division of mass and momentum diffusion coefficients is knows as Sc while diffusion of mass particles becomes slow down. This decline in diffusion of particles is happened because of inverse relation between Sc and mass diffusion coefficient. Physically, the solute particles are declined due the definition of Sc. This decline in solute particles becomes slow down due to inclement in diffusion of particles. Hence, diffusion of fluid particles becomes slow down versus large values of Sc. The variation in concentration field is investigated by δ_2 while outcomes regarding concentration versus δ_2 is displayed by Fig. 13. It is noticed that δ_2 in dimensionless concentration equation is modeled due to the influence of non-Fourier's law. The diffusion of solute particles for the case of (appearance of Cattaneo–Christov law) is higher than diffusion of solute particles for the case of (disappearance of Cattaneo–Christov law). So, the performance of concentration in the absence of δ_2 is much better than for the case of non-Fourier's law. So, higher values of δ_2 make the reduction in profiles of concentration. It is noticed that δ_2 has analog versus the Deborah number and the fluid has ability to return original state elated to concentration in the fluid. Figure 14 captures the character of ϵ_2 on diffusion of fluid particles. The graph between the diffusion of fluid particles and ϵ_2 is increasing. In this relation, diffusion of fluid particles becomes fast while ϵ_2 is appeared due to variable concentration. Further, this increment in diffusion of fluid particles because ϵ_2 exists as a direct relation versus concentration. So, this direct relation brings increment in diffusion of fluid particles (Figs. 2, 3, 4, 5, 6, 7, 8, 9, 10, 11, 12, 13, 14).

Simulations of divergent velocities against physical parameters. The related simulations of divergent velocities versus the variation of Pr and α are calculated by Tables 2 and 3. The improvement in divergent velocities in y-and x-directions versus the increment in Prandtl number is investigated. Hence, α makes great impact for the enhancement of shear stresses in y-and x-directions. It is also investigated that validation of numerical simulations is done through considered values 0.0, 0.25, 0.5, 0.75 and 1.0 of α with already published work of Wang[27], Kumar et al.[28] and Hayat et al.[29]. The remarkable comparison is found between present work and published results. Temperature gradient versus the various values of Pr is captured by Table 3. From this table, temperature gradient is enhanced with respect to large values of Pr whereas comparison of results are estimated by published work of Khan et al.[30] and Bilal et al.[31] by considering range of Pr ($0.07 \leq Pr \leq 2.0$).

Concluding key points

The numerical simulations of mass and heat energy using conservation laws under the action of non-Fourier's law are numerically solved. The concept of variable properties in view of concentration and thermal conductivity in the presence of Prandtl fluid past a hot surface is considered. The outcomes against the physical parameters are concluded which are listed below:

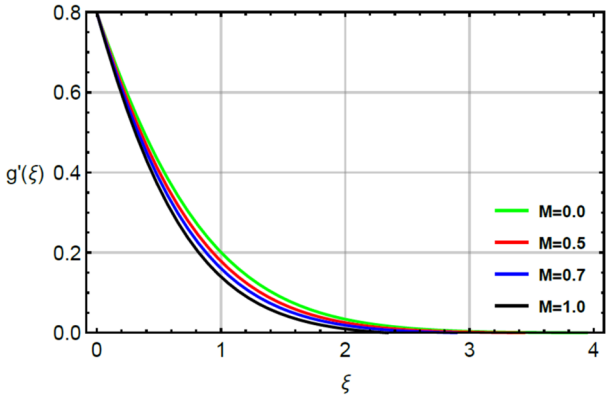

Figure 5. Character of M on g'.

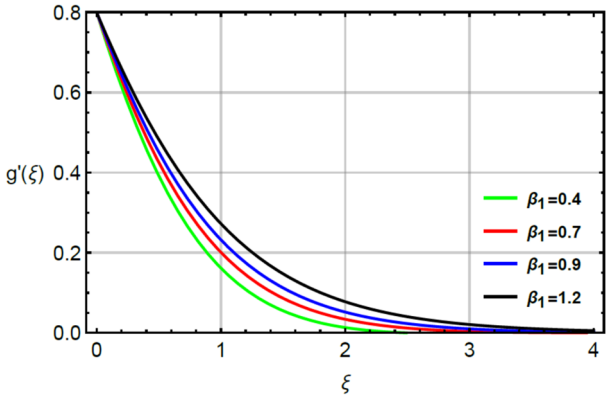

Figure 6. Character of β_1 on g'.

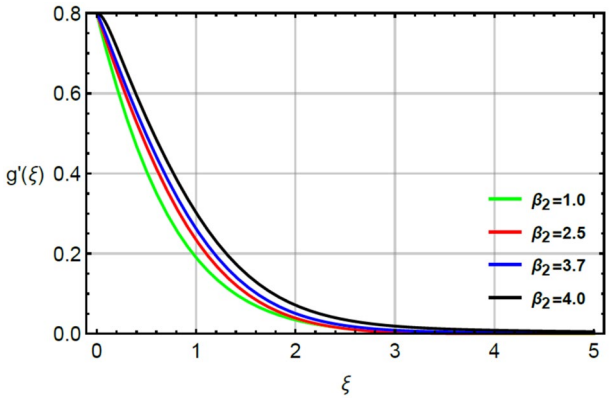

Figure 7. Character of β_2 on g'.

- The magnetic field generates retardation force in motion of fluid particles and MBL (momentum boundary layers) become thick due to retardation force in y- and x-directions of the surface;
- The motion of fluid particles become fast in y- and x-directions of the hot surface by considering the enhancement in Prandtl, ratio and elastic parameters whereas thickness of momentum boundary layers are reduced using large values of Prandtl, ratio and elastic parameters;
- The less production of thermal energy is achieved versus variation in Pr and δ_1. The maximum heat energy is achieved for the case generalized Fourier's law as compared for the case of non- Fourier's law. Prandtl number makes vital impact for adjustment in TBL as well as in MBL;

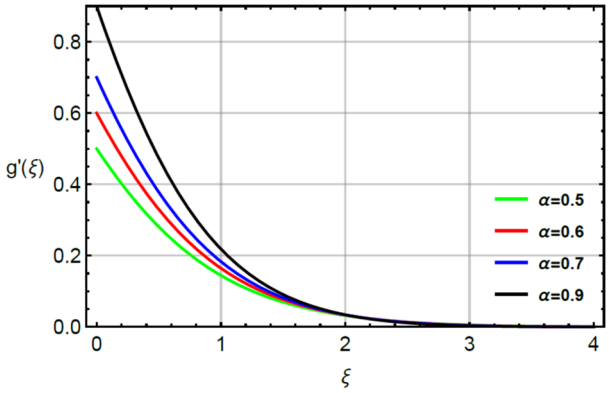

Figure 8. Character of α on g'.

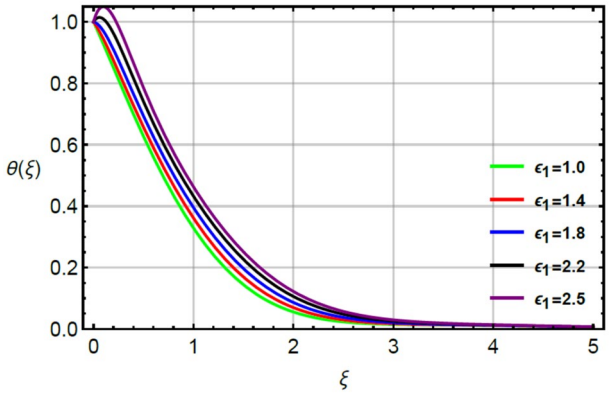

Figure 9. Character of ϵ_1 on θ.

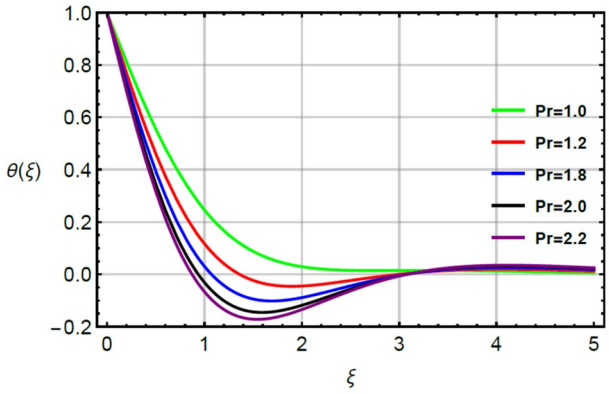

Figure 10. Character of Pr on θ.

- The maximum production of heat energy is obtained for the large values of ϵ_1. Hence, ϵ_1 plays a vital role for maximum production of heat energy;
- The diffusion of fluid particles becomes fast versus the enhancement of ϵ_1. But diffusion of fluid particles becomes slow down versus large values of Sc and δ_2;
- The divergent velocities in y- and x-directions are decreased by the large values of ratio number and gradient temperature is enhanced due to variation in Prandtl number.

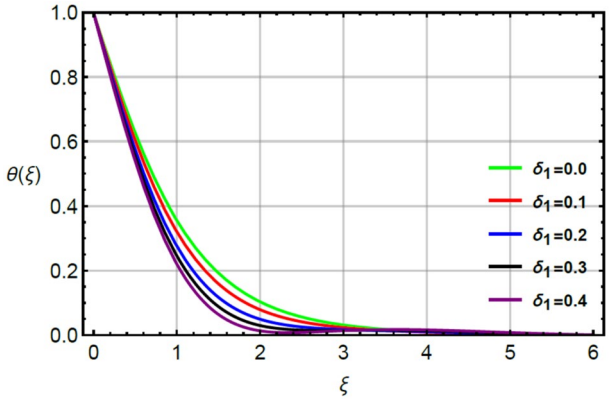

Figure 11. Character of δ_1 on θ.

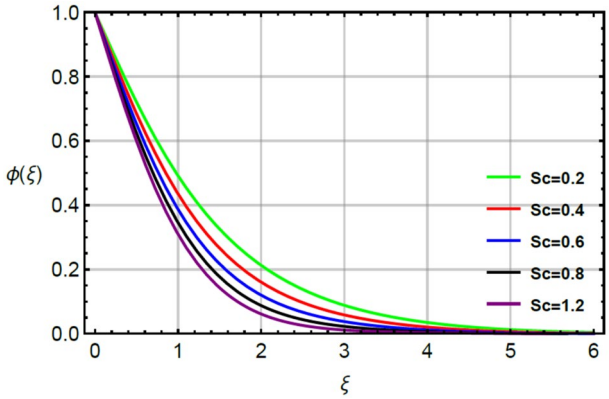

Figure 12. Character of Sc on ϕ.

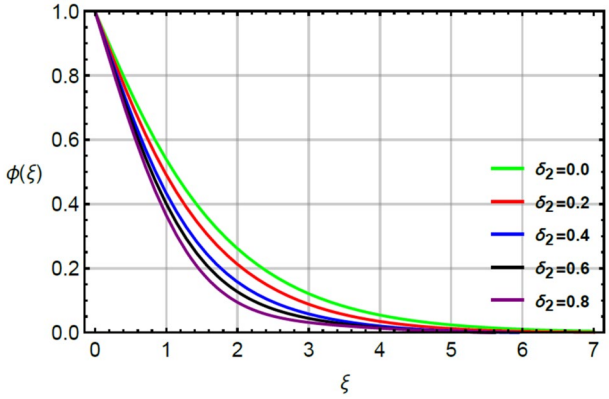

Figure 13. Character of δ_2 on ϕ.

- The solution approach is called HAM analysis scheme is used to simulate the solution of present complex model while current analytical approach is very useful and it has many applications in industrial and engineering processes;
- The significant applications of current model are used in recovery of petroleum, enhancement of heat energy, food making process, energy devices and adjusting cooling devices etc.

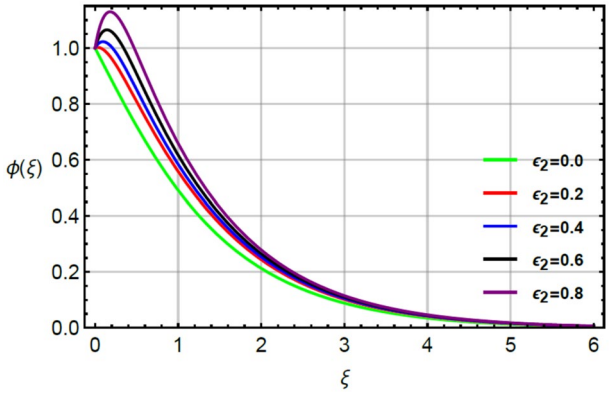

Figure 14. Character of ϵ_2 on ϕ.

	Hayat et al.[29]		Wang[27]		Kumar et al.[28]		Present results	
α	$-f''(0)$	$-g''(0)$	$-f''(0)$	$-g''(0)$	$-f''(0)$	$-g''(0)$	$-f''(0)$	$-g''(0)$
0.0	1.0	0.0	1.0	0.0	1.0	0.0	1.00000	0.000000
0.25	1.048810	0.19457	1.0488	0.1945	1.04906	0.19457	1.048124	0.194562
0.5	1.093095	0.465205	1.0930	0.4652	1.09324	0.46532	1.093054	0.465281
0.75	1.134500	0.794620	1.1344	0.7946	1.13458	0.79470	1.1345012	0.794624
1.0	1.173721	1.173721	1.1737	1.1737	1.17378	1.17378	1.173210	1.173210

Table 2. Comparative analysis of dimensionless stress by fluctuating the values of velocity rates parameter and setting $M = 0$.

Pr	Khan et al.[30]	Bilal et al.[31]	Present Results
0.07	0.06633	0.0660	0.066847
0.20	0.1691	0.1691	0.1697304
0.70	0.4539	0.5349	0.453721
2.00	0.9113	0.9114	0.911708

Table 3. Computation of heat temperature rate for ($g = 0$; i.e. two diemsional case) against Prandtl number by fixing other parameters.

Data availability

The data used to support this study are included in the article.

Received: 7 June 2021; Accepted: 27 July 2021
Published online: 08 September 2021

References

1. Hamid, M., Zubair, T., Usman, M., Khan, Z. H. & Wang, W. Natural convection effects on heat and mass transfer of slip flow of time dependent Prandtl fluid. *J. Comput. Design Eng.* **6**(4), 584–592 (2019).
2. Rajesh, R. & Rajasekhara Gowd, Y. Heat and mass transfer analysis on MHD peristaltic Prandtl fluid model through a tapered channel with thermal radiation. *J. Appl. Comput. Mech.* **5**(5), 951–963 (2019).
3. Eldabe, N. T., Moatimid, G. M., ElShekhipy, A. A. & Aballah, N. F. Mixed convective peristaltic flow of Eyring-Prandtl fluid with chemical reaction and variable electrical conductivity in a tapered asymmetric channel. *Heat Transf. Asian Res.* **48**(5), 1946–1962 (2019).
4. Sajid, T., Sabir, Z., Tanveer, S., Arbi, A. & Altamirano, G. C. Upshot of radiative rotating Prandtl fluid flow over a slippery surface embedded with variable species diffusivity and multiple convective boundary conditions. *Heat Transf.* **50**(3), 2874–2894 (2021).
5. Reddy, M. G., Vijayakumari, P., Kumar, K. G. & Shehzad, S. A. Zero-mass flux and Cattaneo–Christov heat flux through a Prandtl non-Newtonian nanofluid in Darcy-Forchheimer porous space. *Heat Transf.* **50**(1), 220–233 (2021).
6. Le, C., Liu, L. & Li, Z. Thermocapillary instabilities in half zone liquid bridges of low Prandtl fluid with non-equal disks under microgravity. *J. Crystal Growth* **560**, 126063 (2021).
7. Ahmad, S., Nadeem, S., Muhammad, N. & Khan, M. N. Cattaneo-Christov heat flux model for stagnation point flow of micropolar nanofluid toward a nonlinear stretching surface with slip effects. *J. Therm. Anal. Calorim.* **143**, 1–13 (2020).

8. Tassaddiq, A. Impact of Cattaneo-Christov heat flux model on MHD hybrid nano-micropolar fluid flow and heat transfer with viscous and joule dissipation effects. *Sci. Rep.* **11**(1), 1–14 (2021).
9. Ahmad, H. *et al.* Approximate Numerical solutions for the nonlinear dispersive shallow water waves as the Fornberg-Whitham model equations. *Results Phys.* **22**, 103907 (2021).
10. Tulu, A. & Ibrahim, W. MHD slip flow of CNT-ethylene glycol nanofluid due to a stretchable rotating disk with cattaneo–christov heat flux model. *Math. Probl. Eng. 2020*.
11. Mabood, F., Imtiaz, M. & Hayat, T. Features of Cattaneo-Christov heat flux model for Stagnation point flow of a Jeffrey fluid impinging over a stretching sheet: A numerical study. *Heat Transf.* **49**(5), 2706–2716 (2020).
12. Ali, B., Naqvi, R. A., Haider, A., Hussain, D. & Hussain, S. Finite element study of mhd impacts on the rotating flow of casson nanofluid with the double diffusion Cattaneo—Christov heat flux model. *Mathematics* **8**(9), 1555 (2020).
13. Khan, U. *et al.* On the Cattaneo-Christov Heat Flux Model and OHAM analysis for three different types of nanofluids. *Appl. Sci.* **10**(3), 886 (2020).
14. Ramana, K. V., Gangadhar, K., Kannan, T. & Chamkha, A. J. Cattaneo–Christov heat flux theory on transverse MHD Oldroyd-B liquid over nonlinear stretched flow. *J. Therm. Anal. and Calorim.* 1–11 (2021).
15. Jakeer, S., Reddy, P. B., Rashad, A. M. & Nabwey, H. A. Impact of heated obstacle position on magneto-hybrid nanofluid flow in a lid-driven porous cavity with Cattaneo-Christov heat flux pattern. *Alex. Eng. J.* **60**(1), 821–835 (2021).
16. Nadeem, S., Ahmad, S. & Muhammad, N. Cattaneo-Christov flux in the flow of a viscoelastic fluid in the presence of Newtonian heating. *J. Mol. Liq.* **237**, 180–184 (2017).
17. Ahmad, S., Nadeem, S., Muhammad, N. & Khan, M. N. Cattaneo–Christov heat flux model for stagnation point flow of micropolar nanofluid toward a nonlinear stretching surface with slip effects. *J. Therm. Anal. Calorim.* **143** (2), (2021).
18. Ahmad, S., Nadeem, S. & Khan, M. N. Mixed convection hybridized micropolar nanofluid with triple stratification and Cattaneo-Christov heat flux model. *Phys. Scr.* **96**(7), 075205 (2021).
19. Ahmad, S. & Nadeem, S. Flow analysis by Cattaneo-Christov heat flux in the presence of Thomson and Troian slip condition. *Appl. Nanosci.* **10**(12), 4673–4687 (2020).
20. Sohail, M. *et al.* Utilization of updated version of heat flux model for the radiative flow of a non-Newtonian material under Joule heating: OHAM application. *Open Phys.* **19**(1), 100–110 (2021).
21. Sohail, M. *et al.* Theoretical and numerical investigation of entropy for the variable thermophysical characteristics of couple stress material: Applications to optimization. *Alex. Eng. J.* **59**(6), 4365–4375 (2020).
22. Sohail, M., Nazir, U., Chu, Y. M., Al-Kouz, W. & Thounthong, P. Bioconvection phenomenon for the boundary layer flow of magnetohydrodynamic Carreau liquid over a heated disk. *Scientia Iranica* (2021).
23. Wong, H. F., Sohail, M., Siri, Z. & Noor, N. F. M. Numerical solutions for heat transfer of an unsteady cavity with viscous heating. *Comput. Mater. Continua* **68**(1), 319–336 (2021).
24. Zubair, T., Usman, M., Ali, U. & Mohyud-Din, S. T. Homotopy analysis method for system of partial differential equations. *Int. J. Mod. Eng. Sci.* **1**(2), 67–79 (2012).
25. Naseem, T., Niazi, N., Ayub, M. & Sohail, M., Vectorial reduced differential transform method for fractional Cauchy–Riemann system of equations. *Comput. Math. Methods*.
26. Raza, R., Sohail, M., Abdeljawad, T., Naz, R. & Thounthong, P. Exploration of temperature-dependent thermal conductivity and diffusion coefficient for thermal and mass transportation in sutterby nanofluid model over a stretching cylinder. *Complexity* (2021).
27. Wang, C. Y. The three-dimensional flow due to a stretching flat surface. *Phys. Fluids* **27**(8), 1915–1917 (1984).
28. Kumar, K. G., Rudraswamy, N. G. & Gireesha, B. J. Effects of mass transfer on MHD three-dimensional flow of a Prandtl liquid over a flat plate in the presence of chemical reaction. *Results Phys.* **7**, 3465–3471 (2017).
29. Hayat, T., Shehzad, S. A. & Alsaedi, A. Three-dimensional stretched flow of Jeffrey fluid with variable thermal conductivity and thermal radiation. *Appl. Math. Mech.* **34**(7), 823–832 (2013).
30. Khan, W. A. & Aziz, A. Double-diffusive natural convective boundary layer flow in a porous medium saturated with a nanofluid over a vertical plate: Prescribed surface heat, solute and nanoparticle fluxes. *Int. J. Therm. Sci.* **50**(11), 2154–2160 (2011).
31. Bilal, S., Rehman, K. U., Malik, M. Y., Hussain, A. & Awais, M. Effect logs of double diffusion on MHD Prandtl nano fluid adjacent to stretching surface by way of numerical approach. *Results Phys.* **7**, 470–479 (2017).

Acknowledgements

Researchers Supporting Project Number (RSP-2021/33), King Saud University, Riyadh, Saudi Arabia.

Author contributions

U.N., M.S. and U.A. developed the model and write up the modelling section. U.N., C.P. draw the graphs. U.N. prepared figure. Introduction section is updated by E-S.M.S., C.P., J.R.L. in the revised draft. E-S.M.S., C.P., J.R.L., confirms the modelling and helped in the literature survey. Results and discussion section is improved by M.S., M.M.S. and P.T. M.M.S. and P.T. write the discussion section of the article. Conclusion section is updated by E-S.M.S., C.P., J.R.L. The authors order have been corrected. All the authors approved the revised version.

Competing interests

The authors declare no competing interests.

Additional information

Correspondence and requests for materials should be addressed to M.S. or C.P.